Neurobiology of Aging 126 (2023) 67–76

Contents lists available at ScienceDirect

Neurobiology of Aging

journal homepage: www.elsevier.com/locate/neuaging.org

Loss of amyotrophic lateral sclerosis risk factor *SCFD1* causes motor dysfunction in *Drosophila*

Rebecca Borg[a,b], Angie Purkiss[a,b], Rebecca Cacciottolo[a,b], Paul Herrera[a,b], Ruben J. Cauchi[a,b,*]

[a] Centre for Molecular Medicine and Biobanking, Biomedical Sciences Building, University of Malta, Msida, Malta
[b] Department of Physiology and Biochemistry, Faculty of Medicine and Surgery, University of Malta, Msida, Malta

ARTICLE INFO

Article history:
Received 21 September 2022
Revised 13 February 2023
Accepted 15 February 2023
Available online 21 February 2023

Keywords:
Amyotrophic lateral sclerosis
Drosophila
SCFD1
Sly1
Slh

ABSTRACT

Amyotrophic lateral sclerosis (ALS) is a progressive neuromuscular disease mostly resulting from a complex interplay between genetic, environmental and lifestyle factors. Common genetic variants in the *Sec1 Family Domain Containing 1* (*SCFD1*) gene have been associated with increased ALS risk in the most extensive genome-wide association study (GWAS). *SCFD1* was also identified as a top-most significant expression Quantitative Trait Locus (eQTL) for ALS. Whether loss of SCFD1 function directly contributes to motor system dysfunction remains unresolved. Here we show that moderate gene silencing of *Slh*, the *Drosophila* orthologue of *SCFD1*, is sufficient to cause climbing and flight defects in adult flies. A more severe knockdown induced a significant reduction in larval mobility and profound neuromuscular junction (NMJ) deficits prior to death before metamorphosis. RNA-seq revealed downregulation of genes encoding chaperones that mediate protein folding downstream of *Slh* ablation. Our findings support the notion that loss of *SCFD1* function is a meaningful contributor to ALS and disease predisposition may result from erosion of the mechanisms protecting against misfolding and protein aggregation.

1. Introduction

Amyotrophic lateral sclerosis (ALS) is a neuromuscular disease characterised by progressive loss of motor function culminating in death 3–4 years after clinical onset, typically due to respiratory failure (van Es et al., 2017). A complex interplay between genetic, environment and lifestyle factors is believed to cause the disease in the majority of patients (Vasta et al., 2022). In addition to rare variants that cause familial monogenic forms of the disease, genetic variants that are commonly found in the population have also been associated with disease risk. The latest landmark cross-ancestry genome-wide association study (GWAS) identified several risk loci including *UNC13A* and *SCFD1* (van Rheenen et al., 2021). The relationship of these risk genes with disease mechanism has remained unresolved. However, most recently, 2 compelling studies have demonstrated that for *UNC13A*, mis-splicing of its mRNA transcript in ALS patients eventually results in lower protein levels with dire consequences for synaptic maintenance (Brown et al., 2022; Ma et al., 2022). Although *SCFD1* was also shown to be a top-most significant expression Quantitative Trait Locus (eQTL) for ALS and differential expression was detected in patient-derived motor cortex tissue compared to controls (Iacoangeli et al., 2021), it is presently unknown whether loss of *SCFD1* expression contributes to the pathogenesis of ALS.

While an *in vivo* analysis of SCFD1 function in the neuromuscular system is lacking, the molecular and cellular functions of SCFD1 have been well studied. A member of the Sec1/Munc18-like (SM) protein family, SCFD1 regulates Endoplasmic Reticulum (ER) to Golgi anterograde transport. It does so by ensuring the correct assembly in addition to opposing the disassembly of the soluble N-ethylmaleimide-sensitive factor attachment protein receptor (SNARE) complex, itself required for the fusion of ER-derived vesicles with Golgi membranes (Lobingier et al., 2014; Peng and Gallwitz, 2002). A role for SCFD1 in intra-Golgi and Golgi-to-ER ret-

Abbreviations: ALS, Amyotrophic lateral sclerosis; A5SS, alternative 5' splicing site; A3SS, alternative 3' splicing site; COG, conserved oligomeric Golgi; DEGs, differentially expressed genes; DSGs, differentially spliced genes; eQTL, expression Quantitative Trait Locus; FDR, false discovery rate; GO, Gene Ontology; GWAS, genome-wide association study; HSP, heat shock protein; IMP, inosine monophosphate; MXE, mutually exclusive exons; NMJ, neuromuscular junction; PBS, phosphate buffered saline; RI, retained intron; SCFD1, Sec1 Family Domain Containing 1; SE, skipped exon; SNARE, soluble N-ethylmaleimide-sensitive factor attachment protein receptor.

* Corresponding author at: Centre for Molecular Medicine and Biobanking, Biomedical Sciences Building, University of Malta, Msida, Malta.
E-mail address: ruben.cauchi@um.edu.mt (R.J. Cauchi).

0197-4580/$ – see front matter © 2023 Elsevier Inc. All rights reserved.
https://doi.org/10.1016/j.neurobiolaging.2023.02.005

rograde transport has also been proposed due to a direct interaction with the conserved oligomeric Golgi (COG) tethering complex (Laufman et al., 2009). Impairment of these functions by depletion of SCFD1 in mammalian cells induces an ER stress response that leads to autophagy (Renna et al., 2011). To date, however, studies on animal models with complete or conditional SCFD1 function have been limited, which would be critical for assessing whether this gene and its product play a crucial role in maintaining the motor system *in vivo*.

Here we report on the use of RNAi-mediated gene silencing in the *Drosophila* model system to investigate the *in vivo* consequences of SCFD1 depletion. *Drosophila* has a highly conserved SCFD1 orthologue known as Slh. Adult flies with a moderate deficiency of Slh in either muscle or neurons exhibited motoric deficits. A stronger knockdown of *Slh* in either tissue induced paralysis in flies at an earlier developmental stage as demonstrated by a severe reduction in the larval contraction rate and high puparial axial ratios. This phenotype was accompanied by defects in the neuromuscular junction (NMJ) between the innervating motor neurons and muscle. Transcriptome analysis revealed several alterations that can explain the motor dysfunction resulting from *Slh* depletion. Importantly, a general downregulation of protein folding pathways can explain why loss of *SCFD1* function is a meaningful contributor to ALS.

2. Materials and methods

2.1. Flies

Flies were cultured on food consisting of sugar, corn meal, yeast, and agar in plastic vials at an incubation temperature of 25°C under 12 hours day/night cycles. Male flies were used for adult-based assays whereas equal number of male and female flies were used for larval-based assays. The RNAi transgenic construct *Slh-IR^{CO1}* (ID: 3539R-3) was obtained from the *Drosophila* Genetic Resource Centre at the Kyoto Institute of Technology, Kyoto, Japan. The RNAi transgenic constructs *Slh-IR^{CO2}* (ID: 105669), *Slh-IR^{UN1}* (ID: 108778) and *Slh-IR^{UN2}* (ID: 51840) were obtained from the Vienna *Drosophila* Resource Centre, Austria (Dietzl et al., 2007). The *Dcr-2* transgene and the GAL4 drivers were obtained from the Bloomington *Drosophila* Stock Centre (NIH P40OD018537) at Indiana University, USA. Constitutive expression of transgenes was driven by the *Act5C*-GAL4 (ID: 4414) or *da*-GAL4 (ID: 55851) driver. Eye-selective expression was induced by the *GMR*-GAL4 driver (ID: 1104). The *Mef2*-GAL4 (ID: 27390) and *elav*-GAL4 (ID: 458) drivers were employed to induce expression specific to muscle and neurons, respectively. Combination of the various genetic tools was performed according to standard genetic crossing schemes.

2.2. Protein alignment

The DRSC Integrative Ortholog Prediction Tool (DIOPT, https://www.flyrnai.org/diopt) was utilised to determine % amino acid similarity and identity between human SCFD1 (NP_057190.2) and its *Drosophila* orthologue, Slh (NP_001137769.2). Alignment of the 2 proteins was performed by Clustal Omega (EMBL-EBI).

2.3. Motor function assays

For assessment of larval mobility, third instar (L3) larvae of the appropriate genotype were first placed on a 0.7% agar plate and allowed to acclimatise. Subsequently, the number of forward body wall contractions exhibited by the organism in 30 seconds were counted. Each larva was assessed 3 times before an average was taken. A minimum of 15 larvae were assayed per genotype. Larvae were assessed at 72 hours (L3a) and 96 hours (L3b) after egg laying. To assess climbing performance in adult flies, 2 empty polystyrene tubes were vertically joined by tape facing each other. Flies (15–20) were then transferred into the lower tube and allowed to acclimatise. Flies were then gently tapped down to the bottom of the tube. The number of flies per group that can climb above the 8 cm mark by 10 seconds, was next determined. For each group of flies, 4 trials were performed. A minimum of 4 groups were assayed per genotype. Assessment of flight performance relied on the use of the Droso-Drome apparatus described previously (Cacciottolo et al., 2019). This consisted of a 1 L glass bottle coated with an alcohol-based sticky fluid, and divided into 4 sectors, of 5 cm each, spanning a total height of 20 cm. In short, flies first underwent a "warm-up" by inducing negative geotaxis in an empty tube for 6 times. Organisms were then dropped into the Droso-Drome to induce flight. The number of flies stuck to each sector was next counted, divided by the total number of flies dropped and multiplied by 100 to generate the percentage number of flies per sector. Fight ability correlates with the sector in which flies are distributed on landing, hence, fly percentages that are skewed towards the lower sectors of the Droso-Drome are indicative of reduced flight capacity. Four trials were performed for each group of flies and a minimum of four groups were assayed per genotype.

2.4. Puparial axial ratios

Length and width of puparia were first measured from still images. Calculation of puparial axial ratios involved dividing the length by the width of the puparia as described previously (Cacciottolo et al., 2019).

2.5. Immunohistochemistry

Wandering L3 larvae were dissected in phosphate buffered saline (PBS) to expose the body wall muscles, then fixed in 4% paraformaldehyde in PBS and washed in PBS + 0.1% Triton X-100 (PBT). Tissues were then stained overnight at room temperature by mouse anti-Discs large antibody (1:1000; Developmental Studies Hybridoma Bank, University of Iowa, USA). On the following day, tissues were washed in PBT and stained over-night at room temperature with anti-mouse Alexa Fluor 488-conjugated secondary goat antibody (1:50). After a final wash in PBT, the samples were mounted in 90% glycerol with anti-fade. Imaging was performed with the Optika B-600TiFL microscope (20x or 40x objectives) using brightfield and fluorescent light channels.

2.6. Analysis of NMJ morphology

The area of NMJs innervating ventral longitudinal muscles 6 and 7 derived from abdominal segments 2–3 were quantified by the ImageJ software (NIH). Branch number was determined by counting the number of arborisations containing at least 2 boutons within a single NMJ. To determine bouton numbers, all boutons were counted within a single NMJ.

2.7. RNA extraction

RNA was extracted from 12 to 15 L3 larvae of the desired genotype using the Qiagen RNeasy Plus Mini Kit (Qiagen, Hilden, Germany) following manufacturer's instructions. In brief, whole larvae were homogenized and lysed. Tissue lysates were then spun through genomic DNA eliminator spin columns to remove genomic DNA and RNeasy Mini spin columns were subsequently used to purify total RNA.

2.8. Quantitative RT-PCR

Quantification of *Slh* expression levels was achieved by amplifying the corresponding cDNA using the SOLIScript 1-step SolisGreen kit (Solis Biodyne, Tartu, Estonia) following manufacturer's instructions. The primers were from Integrated DNA Technologies (Leuven, Belgium) and were specific for *Slh* (forward: 5' – TCAGAAGGACGGGCTAAAGA – 3'; reverse: 5' – CGAGAAGTCCTGCTGAATCC – 3') and housekeeping gene *RpL32* (forward: 5' – TACAGGCCCAAGATCGTGAA – 3'; reverse: 5' – GACAATCTCCTTGCGCTTCT – 3'). The transcriptional levels were calculated by the $2-\Delta\Delta Ct$ (Ct, cycle of threshold) method. $\Delta\Delta Ct = \Delta Ct$ of experimental group – mean ΔCt of control groups. $\Delta Ct = Ct$ (gene of interest) – Ct (housekeeping).

2.9. RNA-seq and data analysis

RNA-seq libraries from RNA samples (derived from female L3 larvae) were prepared and sequenced at the Beijing Genomics Institute, Denmark. Briefly, poly(A) mRNA was enriched using poly(T) oligo-attached magnetic beads. This was followed by fragmentation and subsequent first strand cDNA synthesis using random hexamer N6 primers and reverse transcriptase. Following end repair and adaptor ligation, cDNA fragments were PCR amplified and purified to generate single-stranded DNA circles in a final library. DNA nanoballs were finally generated by rolling circle replication, which underwent paired end sequencing (100 bp) on the BGI DNBseq platform.

Raw reads were filtered using SOAPnuke (Li et al., 2009) and clean reads were mapped to the reference *Drosophila* genome using HISAT2 (Kim et al., 2019). Transcript quantification was obtained using RSEM and normalized as fragments per kilobase of transcript per million mapped reads (FPKM) (Li and Dewey, 2011). Differentially expressed genes (DEGs) were identified by the DESeq2 algorithm with *p*-values adjusted for multiple comparisons by the Benjamini and Hochberg procedure, and differential expression of the genes determined using a false discovery rate (FDR) cut off of <0.05 (Love et al., 2014). DEGs with a >2 fold change (log2FC > 1) were selected. Differentially spliced genes (DSGs) were detected using rMATS (Shen et al., 2014) and 5 types of alternative splicing events including skipped exon (SE), alternative 5′ splicing site (A5SS), alternative 3′ splicing site (A3SS), mutually exclusive exons (MXE) and retained Intron (RI) were defined. GO biological pathway analysis on upregulated or downregulated DEGs and DSGs was carried out using ShinyGO (Ge et al., 2020).

2.10. Statistical analysis

Values are presented as means ± S.E.M. unless otherwise indicated. Two-way ANOVA, followed by Dunnett's *post hoc* test, was used for multiple comparisons with control (GraphPad Prism v9.4.1). Differences were deemed statistically significant if $p < 0.05$.

3. Results

3.1. Knockdown of Slh, the Drosophila SCFD1 orthologue

The only predicted orthologue of SCFD1 in *Drosophila* is Slh (CG3539) which is highly conserved throughout its entire length (Fig. 1A). Thus, compared to its human counterpart, Slh has an amino acid similarity and identity of 76% and 57%, respectively (98% coverage). To determine the requirements of Slh in the whole organism or in specific tissues we employed the *UAS*/GAL4 system to activate 4 different RNAi transgenes targeting different regions of the sole 2 predicted *Slh* mRNA transcripts (Fig. 1B). Constitutive expression (*Act5c*-GAL4) of RNAi constructs directed at the 5' coding region, halts developmental progression, thus leading to death either at the third instar larval stage (*Slh-IR^{CO2}*) or even prior (*Slh-IR^{CO1}*). Selective expression of either transgene in neurons (*elav*-GAL4) leads to adult viable flies or death at the pupal stage when knockdown was enhanced with co-expression of the *Dcr-2* transgene (Fig. 1C). When expression was restricted to muscle (*Mef2*-GAL4), flies perished at the pupal stage or at the earlier third instar larval (L3) stage on enhanced knockdown in case of the *Slh-IR^{C01}* RNAi line. Eye-specific expression (*GMR*-GAL4) of the *Slh-IR^{CO2}* or *Slh-IR^{CO2}* transgene, however, does not lead to a rough eye phenotype excluding generic toxicity associated with strong *Slh* knockdown (Supplementary Fig. 1). Either constitutive or tissue-specific activation of the RNAi transgenes targeting the 3' untranslated regions (*Slh-IR^{UN1}* and *Slh-IR^{UN2}*) leads to viable adult flies (Fig. 1C).

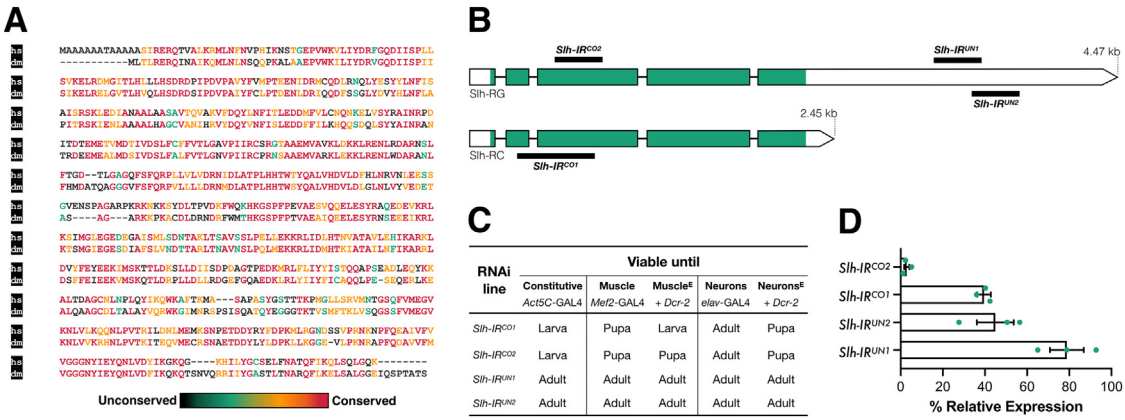

Fig. 1. Viability outcomes and residual expression on activation of RNAi transgenes targeting *Slh*. (A) Protein alignment of human (hs) SCFD1 and its *Drosophila* orthologue (ds) indicating high evolutionary conservation of amino acids throughout the entire protein length. (B) Predicted *Slh* transcripts in *Drosophila* and regions targeted by RNAi constructs. *Slh-IR^{C01}* and *Slh-IR^{CO2}* target the 5' coding region whereas *Slh-IR^{UN1}* and *Slh-IR^{UN2}* target the 3' untranslated region. (C) Viability outcomes of flies in which different RNAi transgenes were driven by the indicated GAL4 drivers either constitutively or selectively in muscle or neurons. *Dcr-2* was co-expressed to enhance tissue-specific knockdown as indicated by E in superscript. (D) *Slh* expression relative to the housekeeping *RpL32* gene in L3b larvae in which the indicated RNAi transgene was constitutively activated (except for *Slh-IR^{C01}* which was selectively driven in muscle) as determined by qRT-PCR. Each bar represents the mean ± SEM of three biological replicates with the respective data points superimposed on the bars.

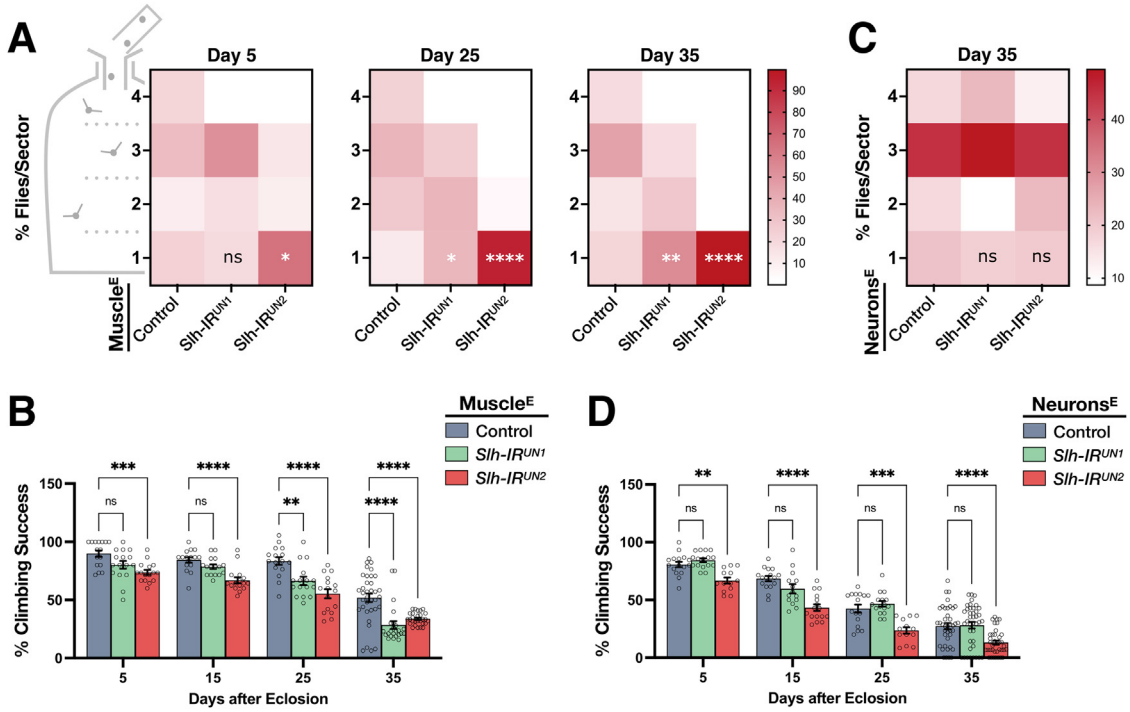

Fig. 2. Knockdown of *Slh* induces motor deficits. (A) Heat maps comparing distribution of flies landing in either of four sectors (4, top; 1, bottom) in differently aged flies with enhanced muscle-selective expression of the indicated RNAi transgenes compared to control (n = 60-300/genotype). (B) Climbing ability of adult flies with enhanced muscle-selective knockdown of *Slh* compared to control and assessed at different time points (n = 60-300/genotype). (C) Heat map showing percentage of flies per sector for old flies with enhanced expression of the indicated RNAi transgenes in neurons compared to control (n = 300/genotype). (D) Climbing ability of differently aged flies with enhanced reduction of *Slh* in neurons compared to control (n = 60-300/genotype). For graphs, each bar represents the mean ± SEM of several independent experiments superimposed on the bars. *Dcr-2* was co-expressed to enhance tissue-specific knockdown as indicated by E in superscript. Significance was tested by two-way ANOVA with Dunnett's *post hoc* test and for all data, *ns* = not significant, $^{*}p = 0.01$, $^{**}p < 0.01$, $^{***}p < 0.001$, and $^{****}p < 0.0001$.

3.2. Correlation between residual Slh expression and viability outcomes

Aiming at correlating the relative residual *Slh* expression levels with viability outcomes, we assessed gene knockdown efficiency by performing quantitative RT-PCR on RNA extracted from L3 larvae with constitutive expression of each transgenic construct. We observed an expression gradient that correlates well with phenotypic severity. Hence, RNAi transgenes derived from non-coding sequences only induced a mild to moderate reduction in *Slh* transcript expression (21%, *Slh-IR*^{UN1}; 55%, *Slh-IR*^{UN2}) (Fig. 1D) and this is compatible with life. Stronger reductions that correlated well with lethality prior to the adult stage were observed upon induction of constructs targeting coding sequences, specifically 97% for *Slh-IR*^{CO2} and 60% for *Slh-IR*^{CO1}. The latter is however a conservative estimate considering that for comparative purposes and, in view of earlier lethality on constitutive transgene activation, gene expression analysis was performed on whole L3 larvae in which gene silencing was only exclusive to muscle tissue whilst the rest of the organism was wild-type.

3.3. Motor impairment in adult flies with loss of Slh function

Given that the RNAi constructs we identified were sufficient to decrease *Slh* expression to varying degrees, we next asked whether reduced levels of Slh leads to an impairment in motor function, which is the most obvious outward feature of ALS. To do so, we generated adult flies with selective knockdown of *Slh* in either muscle or neurons making use of the RNAi constructs associated with a less severe decline in *Slh* transcript abundance. We observed that gene silencing via exclusive expression of *Slh-IR*^{UN2} in muscle induced significant deficits in flight behaviour and climbing ability relative to controls as early as day 5 posteclosion (Fig. 2A,B). Switching to the *Slh-IR*^{UN1} transgene, we show that defects only became apparent later in adulthood in line with its marginal impact on *Slh* levels (Fig. 2A,B). Nonetheless, flies expressing either transgene experienced an age-dependent progressive decline in motor performance. When *Slh* knockdown was directed to neurons, we did not uncover significant flight defects compared to age-matched controls even in aging flies (Fig. 2C). However, whereas flies with neuron-selective activation of *Slh-IR*^{UN1} had normal climbing ability, switching to the stronger *Slh-IR*^{UN2} transgene induced motor dysfunction in young adult flies and a significant deterioration was then observed over time (Fig. 2D).

3.4. A strong Slh deficiency induces muscle contraction and NMJ defects in fly larvae

We wondered whether we can expose severe motor system deficits upon induction of a stronger reduction of *Slh* expression in either muscles or neurons. We first became aware that on pupariation, flies with either muscle- or neuron-specific activation of *Slh-IR*^{CO2} or *Slh-IR*^{CO1} form slender uncontracted puparia (Fig. 3A). Upon quantitation, we note that *Slh* gene silencing directed to either muscle or neurons induced flies to form puparia with significantly higher axial ratios compared to the baseline observed in controls (Fig. 3B). We hypothesised that this phenotype is most probably the consequence of a decline in muscle power experienced by larvae during the earlier L3 stage, hence leading to flies that fail to contract adequately during pupariation. Assessment of

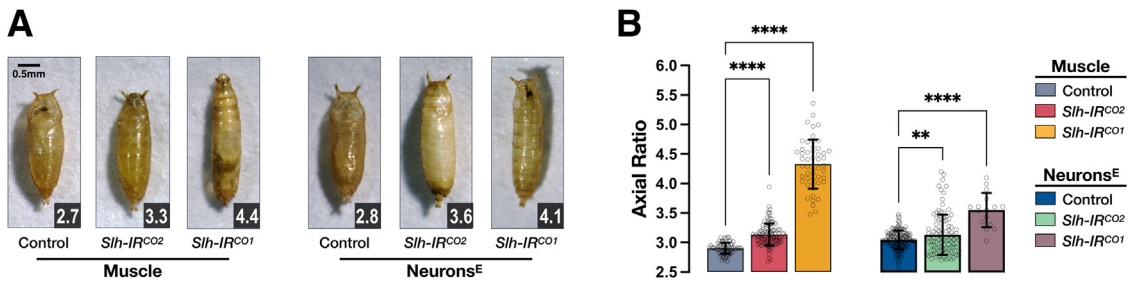

Fig. 3. Loss of *Slh* leads to puparia with high axial ratios. (A) Representative puparia of flies with *Slh* reduction exclusive to either muscle or neurons compared to control. Respective measured ratio is indicated on the right end corner. (B) Puparial axial ratios of flies with muscle- or neuronally-driven *Slh* knockdown compared to respective controls (n = 16-146/genotype). Each bar represents the mean ± SEM of several independent experiments superimposed on the bars. Where indicated, *Dcr-2* was co-expressed to enhance tissue-specific knockdown as indicated by E in superscript. Significance was tested by 2-way ANOVA with Dunnett's *post hoc* test and for all data, $^{**}p < 0.01$, and $^{****}p < 0.0001$.

larval mobility provided confirmation. Therefore, we show that flies with a strong *Slh* knockdown, selective to either component of the neuromuscular system, experienced a significant decline in the larval body wall contraction rate at both the early L3a and late (wandering) L3b stage (Fig. 4A). The effect was most pronounced for flies having muscle-directed *Slh-IR^{CO1}* expression with larvae displaying nearly total immobility, hence appearing rigid and elongated.

We questioned whether we can link the motor deficits observed on loss of *Slh* function with defects in motor synapses, which are a known sign of ALS pathology (Dadon-Nachum et al., 2011; Verma et al., 2022). To this end, we examined NMJs of motor neurons innervating the abdomen of L3 larvae. On visual inspection, we observed that conditional knockdown of *Slh* in either muscle or neurons induced a decrease in NMJ span and complexity (Fig. 4B,C). On quantification, NMJ morphology parameters including area, number of branches and bouton numbers were indeed all profoundly depressed when Slh levels were reduced in muscle or neurons (Fig. 4B,C).

3.5. Transcriptional responses to loss of Slh

Considering that muscle-driven expression of *Slh-IR^{CO1}* induced the most severe motoric ability and synaptic deficits, we carried out RNA sequencing in these larvae to identify molecular changes responsible for these consequences downstream of *Slh* ablation. We found 585 differentially expressed genes (DEGs) of which 302 were downregulated and 283 were upregulated (Fig. 5A, Supplementary Materials Dataset S1). Gene Ontology (GO) analysis was next employed to identify dysregulated pathways. The most highly activated pathways were histone-mediated nuclear processes, immune response and inosine monophosphate (IMP) synthesis (Fig. 5B). Immune-related pathways have also been found altered in ALS animal models and human samples upon similar transcriptome investigations (Cao and Scotter, 2022; D'Erchia et al., 2017; Eshima et al., 2023; Humphrey et al., 2023; Liu et al., 2019). Intriguingly, we reveal that the most significantly down-regulated pathways revolved around protein folding or refolding (Fig. 5C). Hence, several genes that encode heat shock proteins (HSPs) all had their expression significantly depressed with *Hsp70Aa, Hsp70Bbb,* and *Hsp70Ba* ranking amongst the top 20 genes with the highest fold change (Fig. 5A, Supplementary Materials Dataset S1).

Considering that gene expression is also influenced by splicing alterations we examined the genes that were differentially spliced upon *Slh* gene silencing. Our analysis revealed 170 differentially spliced genes (DSGs), of which 37 had an alternative 3' splice site (A3SS), 48 had an alternative 5' splice site (A5SS), 25 had a mutually exclusive exon (MXE), 54 had a retained intron (RI), and 52 had a skipped exon (SE). Several transcripts were subjected to more than one mode of alternative splicing, and the transcript encoded by the polyubiquitin gene *Ubi-p63E* (*CG11624*) was affected by all modes (Fig. 6A, Supplementary Materials Dataset S2). GO biological pathway analysis on DSGs revealed an enrichment of terms associated with muscle development and structure including actin filament assembly within the muscle myofibril (Fig. 4B). Several genes involved in these processes were all found alternatively spliced downstream of *Slh* loss (Table 1).

4. Discussion

SCFD1 has been previously identified as an ALS risk gene via analysis of GWAS and eQTL data (Iacoangeli et al., 2021; van Rheenen et al., 2016; van Rheenen et al., 2021). Prior to our study, it has remained unresolved whether a factor involved in ER-Golgi trafficking is necessary for maintaining a functional motor system *in vivo* and how loss of *SCFD1* expression could increase ALS risk. We attempted to address these questions by inducing RNAi-mediated gene silencing of the highly conserved *SCFD1* orthologue *Slh* in flies. Our findings demonstrate that, indeed, loss of *Drosophila Slh* is sufficient to replicate some aspects of ALS disease phenotypes and pathology *in vivo* including severe impairment in motor behaviour and profound NMJ deficits. This underscores that vesicle transport is central to the physiology of the neuromuscular system and is supported by the discovery of an increasing number of ALS-associated genes that play a role in this pathway including *SPG11, VABP, ALS2*, *FIG4*, *CAV1, OPTN, UNC13A*, and *NEK1* (Mead et al., 2022). Transcriptome profiling also revealed that *Slh* gene silencing leads to a highly-significant depression in pathways associated with chaperone-mediated protein folding, which hints at a plausible mechanism through which reduction in SCFD1 levels may predispose to ALS.

Misfolding and protein aggregation is a hallmark feature of ALS (Parakh and Atkin, 2016). In the majority of patients with ALS, TDP-43 is the main constituent of protein aggregates, although mutations in *TARDBP*, its encoding gene, are a rare cause of ALS (Scotter et al., 2015). Other types of protein aggregates might be observed in specific subtypes of ALS including inclusions containing dipeptide repeat proteins associated with *C9orf72* mutations and SOD1 or FUS aggregates in patients harbouring *SOD1* or *FUS* mutations, respectively (Hardiman et al., 2017). Downregulation of HSPs can therefore explain why a reduction in SCFD1 levels can lead to a cellular environment that is prone to accumulation of malformed proteins. HSPs act as chaperones by recognising and binding misfolded proteins to either promote their refolding or induce degradation (Janowska et al., 2019). Reduced levels of HSPs have been reported in ALS animal models and in ALS patient-

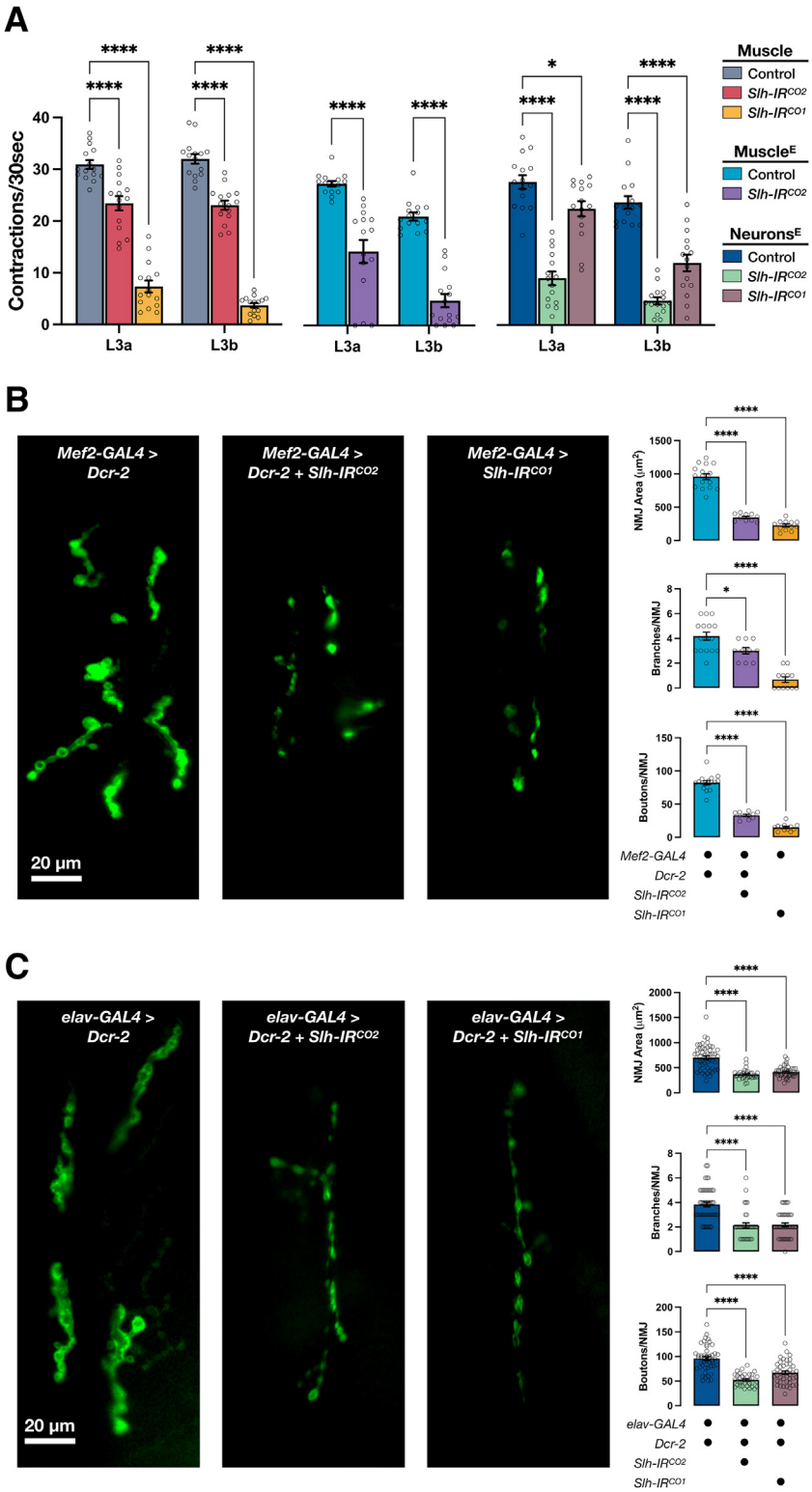

Fig. 4. RNAi-mediated silencing of *Slh* leads to paralysis and NMJ deficits in fly larvae. (A) Velocity of L3a and late (wandering) L3b larvae in which *Slh* was silenced in muscle or neurons (n =15/genotype). Enhanced knockdown was achieved by co-expression of *Dcr-2* as indicated by E in superscript. (B) *Left*, Representative DLG-stained NMJs innervating ventral longitudinal muscles 6 and 7 in L3b larvae with *Slh* reduction exclusive to muscle compared to control (n = 10-16 larvae). *Right*, Quantification of NMJ area, number of branches per NMJ and number of boutons per NMJ in larvae with muscle-driven *Slh* knockdown compared to control (n = 10-16 NMJs/genotype). (C) *Left*, Representative DLG-stained NMJs innervating ventral longitudinal muscles 6 and 7 in L3b larvae with *Slh* reduction exclusive to neurons compared to control (n = 16-24 larvae). *Right*, Quantification of NMJ area, number of branches per NMJ and number of boutons per NMJ in larvae with neuronally-driven *Slh* knockdown compared to control (n = 35–48 NMJs/genotype). For graphs, each bar represents the mean ± SEM of several independent experiments superimposed on the bars. Significance was tested by 2-way ANOVA with Dunnett's *post hoc* test and for all data, $^{*}p = 0.01$, $^{**}p < 0.01$, $^{***}p < 0.001$, and $^{****}p < 0.0001$.

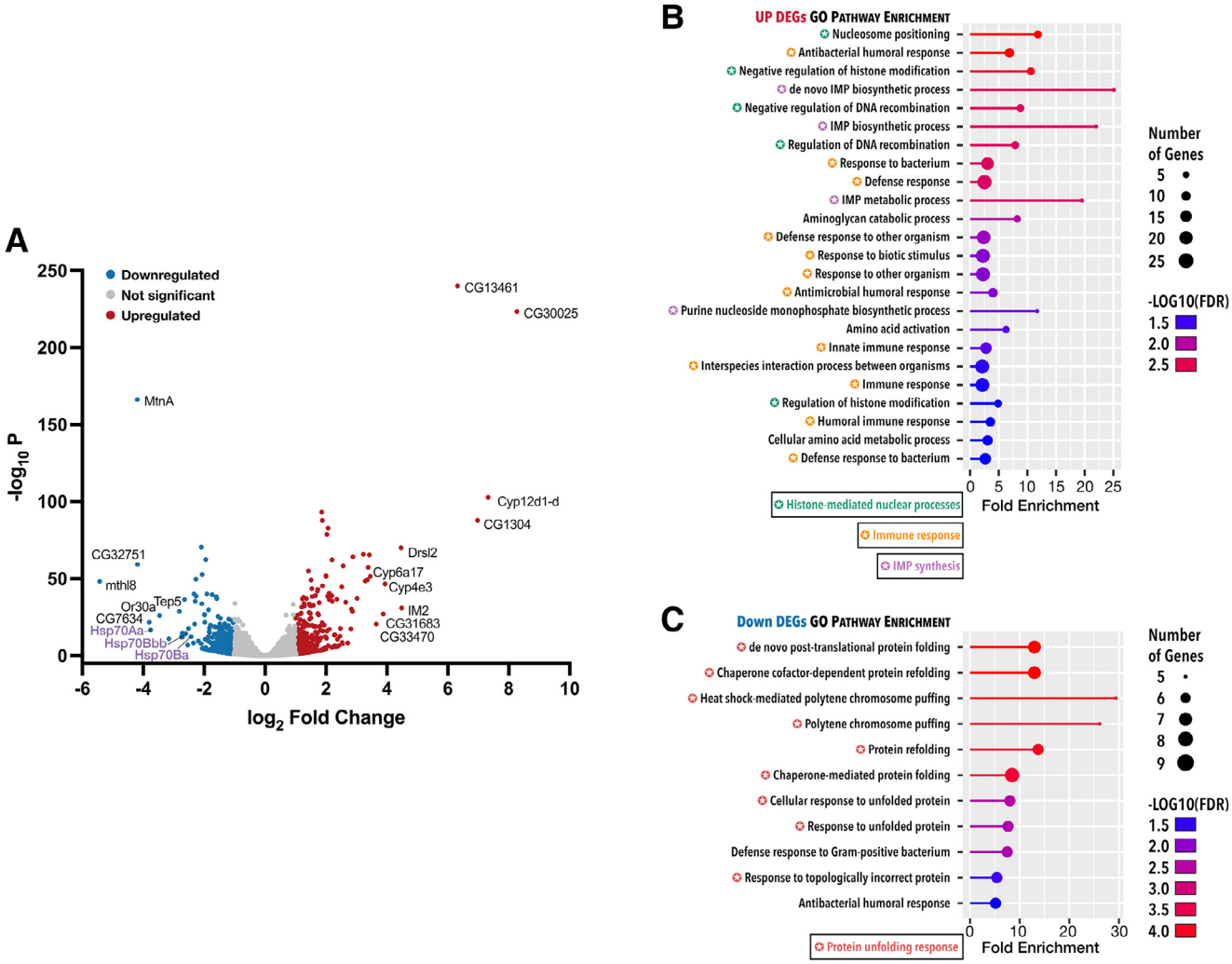

Fig. 5. Analysis of genes with expression changes in response to *Slh* gene silencing. (A) Volcano plot showing differentially expressed genes (DEGs) in L3b larvae with muscle-selective *Slh-IR*^{CO1} activation compared to the driver only control ($n = 3$ biological replicates, sex = females). Topmost significant DEGs are annotated including those encoding heat shock proteins (purple). (B) Lollipop plot presenting significant biological process terms enriched in upregulated DEGs upon gene ontology (GO) analysis. (C) Lollipop plot presenting significant biological process terms enriched in downregulated DEGs upon gene ontology (GO) analysis. In B–C, GO terms are sorted by FDR (<0.05) with the colour of the lollipops representing the values of the enrichment analysis relative to the other displayed terms (brighter red is more significant) and the size of the dots represent the number of genes that comprise the term. GO terms tagged with a colour-coded star indicate pathway overlap.

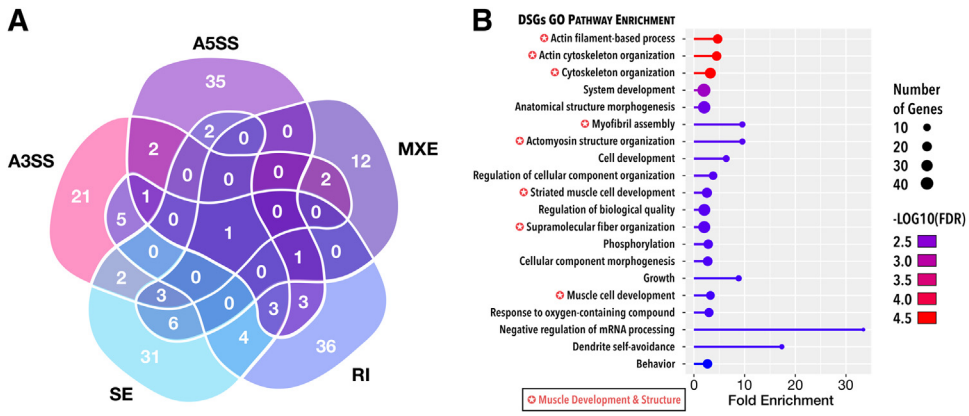

Fig. 6. Analysis of genes with splicing alterations in response to *Slh* gene silencing. (A) Venn diagram showing overlap of differentially spliced genes (DSGs) across the five modes of alternative splicing including alternative 3' splice site (A3SS), alternative 5' splice site (A5SS), mutually exclusive exon (MXE), retained intron (RI) and skipped exon (SE). (B) Lollipop plot exhibiting the top-most 20 significant GO biological process terms enriched in DSGs. GO terms are sorted by FDR (<0.05) with the colour of the lollipops representing the values of the enrichment analysis relative to the other displayed terms (brighter red is more significant) and the size of the dots represent the number of genes that comprise the term. GO terms tagged with a colour-coded star indicate pathway overlap.

Table 1
Genes involved in muscle development and myofibril assembly that are alternatively spliced downstream of *Slh* loss of function

Gene	Protein	Alternative Splicing Events	Function
Actn	α-actinin	A3SS	Enables actin filament binding assembly and sarcomere organisation
Sals	sarcomere length short	RI	Actin binding protein that promotes sarcomeric actin filament elongation from pointed ends during muscle growth
Mical	Molecule interacting with CasL	MXE, SE	Enzyme that inhibits actin polymerisation
C3G	C3G guanyl-nucleotide exchange factor	RI	Plays a role in body wall muscle development during larval stages
Mhc	Myosin heavy chain	A3SS, MXE, SE	A motor protein that provides the force for muscle contraction through its ATP-dependent interaction with actin filaments.
Zasp52	Z band alternatively spliced PDZ-motif protein 52	MXE, SE	A scaffold protein that binds to α-actinin and localizes to muscle attachment sites and Z-discs in muscle cells

Key: A3SS, alternative 3' splice site; MXE, mutually exclusive exon; RI, retained intron; SE, skipped exon.

derived tissues or cells (Chen et al., 2016; Filareti et al., 2017; Seminary et al., 2018). Recently, *DNAJC7*, which encodes HSP40 has been identified as a novel ALS-associated gene (Farhan et al., 2019). Importantly, several studies are supportive of an amelioration of ALS symptoms by upregulation of HSPs (Gifondorwa et al., 2007; Kieran et al., 2004; Lin et al., 2013; Novoselov et al., 2013; Sharp et al., 2008). It is still unclear how loss of *SCFD1* function leads to an intrinsic depression of HSPs. Taking into consideration the well-known function of SCFD1 in vesicle transport, it is possible that that the processing of factors controlling HSP expression, including the major stress-sensing transcriptional factor HSF1, is sensitive to defects in the secretory pathway. Alternatively, the upregulation of several histones required for the condensation of chromatin structure as revealed by our transcriptome analysis may have prevented the appropriate expression of protective HSP genes. In a similar vein, TDP-43 was found to impair chromatin remodelling by reducing the recruitment of the chromatin remodeller Chd1 to chromatin also leading to compromised induction of HSP gene expression (Berson et al., 2017). It is well-known that motor neurons and muscle cells are highly inefficient at mounting a heat shock stress response (Batulan et al., 2003; Bhattacharya et al., 2014) and dysregulation of pathways downstream of defective ER-Golgi trafficking can therefore further increase the vulnerability of the motor system to proteome stress.

Our work also shines light on the tissue-specific requirements of Slh. Although a requirement in either muscle or neurons is apparent, our evidence shows that, compared to neurons, muscles are more sensitive to toxicity induced by reduced levels of Slh. We show that alterations in viability, motoric ability and NMJ structure were therefore more severe in organisms in which *Slh* loss of function was restricted to muscle. The transcriptome profile underscores the vulnerability of muscles to *Slh* deficiency. To this end, several genes involved in muscle development and myofibril assembly are incorrectly spliced. Furthermore, an activation of pathways leading to synthesis of IMP is most probably a response to muscle injury since elevated IMP levels due to increased adenine nucleotide degradation, especially ATP, are observed after high-intensity exercise (Bangsbo et al., 2007; Green, 1997; Sahlin et al., 1989) or in disease states and conditions where muscle atrophy is prominent (Miller et al., 2019). In addition to this work, the contribution of muscle to ALS pathophysiology is supported by various studies on animal models (Anakor et al., 2022; Loeffler et al., 2016). Considering *Drosophila*, for instance, muscle-selective disruption of TDP-43 results in motor abnormalities that overlap with those described here (Diaper et al., 2013). Whether ALS originates in skeletal muscle leading to motor neuron death through a retrograde signalling cascade, the so-called “dying-back” hypothesis, remains controversial and highly debatable. However, it is highly likely that non-neuronal cell types including muscle have important roles in the disease process.

We believe that the *Slh* fly models we reported and characterised will be invaluable tools for answering questions raised by this work including the precise mechanisms that drive the transcriptional changes downstream of *Slh* loss of function. Strategies aimed at restricted gene silencing to the adult stage can also inform on whether defects arise during development. In conclusion, our evidence is supportive of the possibility that disruption of SCFD1 function is a likely contributor to ALS. An impairment in the protective response against proteome stress might explain why loss of *SCFD1* increases ALS risk. It is therefore plausible for us to speculate that restoration of SCFD1 expression in ALS patients may be a meaningful therapeutic strategy aimed at improving motor function.

Verification

The submitted work has not been published previously, and it is not under consideration for publication elsewhere. The publication is approved by all authors.

Disclosure statement

The authors declare no competing interest.

CRediT authorship contribution statement

Rebecca Borg: Investigation. **Angie Purkiss:** Investigation. **Rebecca Cacciottolo:** Investigation. **Paul Herrera:** Investigation, Formal analysis, Data curation, Visualization. **Ruben J. Cauchi:** Conceptualization, Methodology, Investigation, Formal analysis, Data curation, Writing – original draft, Writing – review & editing, Visualization, Supervision, Project administration, Funding acquisition.

Acknowledgements

The authors are indebted to Matthew Camilleri for unwavering technical support. For fly stocks, we are grateful to the Vienna *Drosophila* Resource Center (Austria), the National Institute of Genetics Fly Stock Center (Japan) and the Bloomington *Drosophila* Stock Centre (USA). This work was supported by the Malta Council for Science & Technology Fusion R&I Research Excellence Programme, the University of Malta Research Seed Fund, a Tertiary Education Scholarship, and the Anthony Rizzo Memorial ALS Research Fund facilitated by the Research Trust (RIDT) of the University of Malta.

Supplementary materials

Supplementary material associated with this article can be found, in the online version, at doi:10.1016/j.neurobiolaging.2023.02.005.

References

Anakor, E., Duddy, W.J., Duguez, S., 2022. The cellular and molecular signature of ALS in muscle. J. Pers. Med. 12 (11), 1868.

Bangsbo, J., Iaia, F.M., Krustrup, P., 2007. Metabolic response and fatigue in soccer. Int. J. Sports Physiol. Perform 2 (2), 111–127.

Batulan, Z., Shinder, G.A., Minotti, S., He, B.P., Doroudchi, M.M., Nalbantoglu, J., Strong, M.J., Durham, H.D., 2003. High threshold for induction of the stress response in motor neurons is associated with failure to activate HSF1. J. Neurosci. 23 (13), 5789–5798.

Berson, A., Sartoris, A., Nativio, R., Van Deerlin, V., Toledo, J.B., Porta, S., Liu, S., Chung, C.Y., Garcia, B.A., Lee, V.M., Trojanowski, J.Q., Johnson, F.B., Berger, S.L., Bonini, N.M., 2017. TDP-43 promotes neurodegeneration by impairing chromatin remodeling. Curr. Biol. 27 (23), 3579–3590.

Bhattacharya, A., Wei, R., Hamilton, R.T., Chaudhuri, A.R., 2014. Neuronal cells but not muscle cells are resistant to oxidative stress mediated protein misfolding and cell death: role of molecular chaperones. Biochem. Biophys. Res. Commun. 446 (4), 1250–1254.

Brown, A.L., Wilkins, O.G., Keuss, M.J., Hill, S.E., Zanovello, M., Lee, W.C., Bampton, A., Lee, F.C.Y., Masino, L., Qi, Y.A., Bryce-Smith, S., Gatt, A., Hallegger, M., Fagegaltier, D., Phatnani, H., Consortium, N.A., Newcombe, J., Gustavsson, E.K., Seddighi, S., Reyes, J.F., Coon, S.L., Ramos, D., Schiavo, G., Fisher, E.M.C., Raj, T., Secrier, M., Lashley, T., Ule, J., Buratti, E., Humphrey, J., Ward, M.E., Fratta, P., 2022. TDP-43 loss and ALS-risk SNPs drive mis-splicing and depletion of UNC13A. Nature 603 (7899), 131–137.

Cacciottolo, R., Ciantar, J., Lanfranco, M., Borg, R.M., Vassallo, N., Bordonne, R., Cauchi, R.J., 2019. SMN complex member Gemin3 self-interacts and has a functional relationship with ALS-linked proteins TDP-43. FUS and Sod1. Sci. Rep. 9 (1), 18666.

Cao, M.C., Scotter, E.L., 2022. Transcriptional targets of amyotrophic lateral sclerosis/frontotemporal dementia protein TDP-43 - meta-analysis and interactive graphical database. Dis. Model. Mech. 15 (9), dmm049418.

Chen, H.J., Mitchell, J.C., Novoselov, S., Miller, J., Nishimura, A.L., Scotter, E.L., Vance, C.A., Cheetham, M.E., Shaw, C.E., 2016. The heat shock response plays an important role in TDP-43 clearance: evidence for dysfunction in amyotrophic lateral sclerosis. Brain 139 (5), 1417–1432 Pt.

D'Erchia, A.M., Gallo, A., Manzari, C., Raho, S., Horner, D.S., Chiara, M., Valletti, A., Aiello, I., Mastropasqua, F., Ciaccia, L., Locatelli, F., Pisani, F., Nicchia, G.P., Svelto, M., Pesole, G., Picardi, E., 2017. Massive transcriptome sequencing of human spinal cord tissues provides new insights into motor neuron degeneration in ALS. Sci. Rep. 7 (1), 10046.

Dadon-Nachum, M., Melamed, E., Offen, D., 2011. The "dying-back" phenomenon of motor neurons in ALS. J. Mol. Neurosci. 43 (3), 470–477.

Diaper, D.C., Adachi, Y., Lazarou, L., Greenstein, M., Simoes, F.A., Di Domenico, A., Solomon, D.A., Lowe, S., Alsubaie, R., Cheng, D., Buckley, S., Humphrey, D.M., Shaw, C.E., Hirth, F., 2013. Drosophila TDP-43 dysfunction in glia and muscle cells cause cytological and behavioural phenotypes that characterize ALS and FTLD. Hum. Mol. Genet. 22 (19), 3883–3893.

Dietzl, G., Chen, D., Schnorrer, F., Su, K.C., Barinova, Y., Fellner, M., Gasser, B., Kinsey, K., Oppel, S., Scheiblauer, S., Couto, A., Marra, V., Keleman, K., Dickson, B.J., 2007. A genome-wide transgenic RNAi library for conditional gene inactivation in Drosophila. Nature 448 (7150), 151–156.

Eshima, J., O'Connor, S.A., Marschall, E., Consortium, N.A., Bowser, R., Plaisier, C.L., Smith, B.S., 2023. Molecular subtypes of ALS are associated with differences in patient prognosis. Nat. Commun. 14 (1), 95.

Farhan, S.M.K., Howrigan, D.P., Abbott, L.E., Klim, J.R., Topp, S.D., Byrnes, A.E., Churchhouse, C., Phatnani, H., Smith, B.N., Rampersaud, E., Wu, G., Wuu, J., Shatunov, A., Iacoangeli, A., Al Khleifat, A., Mordes, D.A., Ghosh, S., Consortium, A., Consortium, F., Project Min, E.C., Consortium, C.R., Eggan, K., Rademakers, R., McCauley, J.L., Schule, R., Zuchner, S., Benatar, M., Taylor, J.P., Nalls, M., Gotkine, M., Shaw, P.J., Morrison, K.E., Al-Chalabi, A., Traynor, B., Shaw, C.E., Goldstein, D.B., Harms, M.B., Daly, M.J., Neale, B.M., 2019. Exome sequencing in amyotrophic lateral sclerosis implicates a novel gene, DNAJC7, encoding a heat-shock protein. Nat. Neurosci. 22 (12), 1966–1974.

Filareti, M., Luotti, S., Pasetto, L., Pignataro, M., Paolella, K., Messina, P., Pupillo, E., Filosto, M., Lunetta, C., Mandrioli, J., Fuda, G., Calvo, A., Chio, A., Corbo, M., Bendotti, C., Beghi, E., Bonetto, V., 2017. Decreased levels of foldase and chaperone proteins are associated with an early-onset amyotrophic lateral sclerosis. Front. Mol. Neurosci. 10, 99.

Ge, S.X., Jung, D., Yao, R., 2020. ShinyGO: a graphical gene-set enrichment tool for animals and plants. Bioinformatics 36 (8), 2628–2629.

Gifondorwa, D.J., Robinson, M.B., Hayes, C.D., Taylor, A.R., Prevette, D.M., Oppenheim, R.W., Caress, J., Milligan, C.E., 2007. Exogenous delivery of heat shock protein 70 increases lifespan in a mouse model of amyotrophic lateral sclerosis. J. Neurosci. 27 (48), 13173–13180.

Green, H.J., 1997. Mechanisms of muscle fatigue in intense exercise. J. Sports Sci. 15 (3), 247–256.

Hardiman, O., Al-Chalabi, A., Chio, A., Corr, E.M., Logroscino, G., Robberecht, W., Shaw, P.J., Simmons, Z., van den Berg, L.H., 2017. Amyotrophic lateral sclerosis. Nat. Rev. Dis. Primers 3, 17071.

Humphrey, J., Venkatesh, S., Hasan, R., Herb, J.T., de Paiva Lopes, K., Kucukali, F., Byrska-Bishop, M., Evani, U.S., Narzisi, G., Fagegaltier, D., Consortium, N.A., Sleegers, K., Phatnani, H., Knowles, D.A., Fratta, P., Raj, T., 2023. Integrative transcriptomic analysis of the amyotrophic lateral sclerosis spinal cord implicates glial activation and suggests new risk genes. Nat. Neurosci. 26 (1), 150–162.

Iacoangeli, A., Fogh, I., Selvackadunco, S., Topp, S.D., Shatunov, A., van Rheenen, W., Al-Khleifat, A., Opie-Martin, S., Ratti, A., Calvo, A., Consortium, U.K.B.E., Van Damme, P., Robberecht, W., Chio, A., Dobson, R.J., Hardiman, O., Shaw, C.E., van den Berg, L.H., Andersen, P.M., Smith, B.N., Silani, V., Veldink, J.H., Breen, G., Troakes, C., Al-Chalabi, A., Jones, A.R., 2021. SCFD1 expression quantitative trait loci in amyotrophic lateral sclerosis are differentially expressed. Brain. Commun. 3 (4), fcab236.

Janowska, M.K., Baughman, H.E.R., Woods, C.N., Klevit, R.E., 2019. Mechanisms of small heat shock proteins. Cold Spring Harb. Perspect. Biol. 11 (10).

Kieran, D., Kalmar, B., Dick, J.R., Riddoch-Contreras, J., Burnstock, G., Greensmith, L., 2004. Treatment with arimoclomol, a coinducer of heat shock proteins, delays disease progression in ALS mice. Nat. Med. 10 (4), 402–405.

Kim, D., Paggi, J.M., Park, C., Bennett, C., Salzberg, S.L., 2019. Graph-based genome alignment and genotyping with HISAT2 and HISAT-genotype. Nat. Biotechnol. 37 (8), 907–915.

Laufman, O., Kedan, A., Hong, W., Lev, S., 2009. Direct interaction between the COG complex and the SM protein, Sly1, is required for Golgi SNARE pairing. EMBO J 28 (14), 2006–2017.

Li, B., Dewey, C.N., 2011. RSEM: accurate transcript quantification from RNA-Seq data with or without a reference genome. BMC Bioinformatics. 12, 323.

Li, R., Yu, C., Li, Y., Lam, T.W., Yiu, S.M., Kristiansen, K., Wang, J., 2009. SOAP2: an improved ultrafast tool for short read alignment. Bioinformatics. 25 (15), 1966–1967.

Lin, P.Y., Simon, S.M., Koh, W.K., Folorunso, O., Umbaugh, C.S., Pierce, A., 2013. Heat shock factor 1 over-expression protects against exposure of hydrophobic residues on mutant SOD1 and early mortality in a mouse model of amyotrophic lateral sclerosis. Mol. Neurodegener. 8, 43.

Liu, E.Y., Russ, J., Cali, C.P., Phan, J.M., Amlie-Wolf, A., Lee, E.B., 2019. Loss of Nuclear TDP-43 Is Associated with Decondensation of LINE Retrotransposons. Cell. Rep. 27 (5), 1409–1421 e1406.

Lobingier, B.T., Nickerson, D.P., Lo, S.Y., Merz, A.J., 2014. SM proteins Sly1 and Vps33 co-assemble with Sec17 and SNARE complexes to oppose SNARE disassembly by Sec18. Elife. 3, e02272.

Loeffler, J.P., Picchiarelli, G., Dupuis, L., Gonzalez De Aguilar, J.L., 2016. The role of skeletal muscle in amyotrophic lateral sclerosis. Brain. Pathol. 26 (2), 227–236.

Love, M.I., Huber, W., Anders, S., 2014. Moderated estimation of fold change and dispersion for RNA-seq data with DESeq2. Genome. Biol. 15 (12), 550.

Ma, X.R., Prudencio, M., Koike, Y., Vatsavayai, S.C., Kim, G., Harbinski, F., Briner, A., Rodriguez, C.M., Guo, C., Akiyama, T., Schmidt, H.B., Cummings, B.B., Wyatt, D.W., Kurylo, K., Miller, G., Mekhoubad, S., Sallee, N., Mekonnen, G., Ganser, L., Rubien, J.D., Jansen-West, K., Cook, C.N., Pickles, S., Oskarsson, B., Graff-Radford, N.R., Boeve, B.F., Knopman, D.S., Petersen, R.C., Dickson, D.W., Shorter, J., Myong, S., Green, E.M., Seeley, W.W., Petrucelli, L., Gitler, A.D., 2022. TDP-43 represses cryptic exon inclusion in the FTD-ALS gene UNC13A. Nature 603 (7899), 124–130.

Mead, R.J., Shan, N., Reiser, H.J., Marshall, F., Shaw, P.J., 2022. Amyotrophic lateral sclerosis: a neurodegenerative disorder poised for successful therapeutic translation. Nat. Rev. Drug. Discov. 22, 1–28.

Miller, S.G., Hafen, P.S., Brault, J.J., 2019. Increased adenine nucleotide degradation in skeletal muscle atrophy. Int. J. Mol. Sci. 21 (1).

Novoselov, S.S., Mustill, W.J., Gray, A.L., Dick, J.R., Kanuga, N., Kalmar, B., Greensmith, L., Cheetham, M.E., 2013. Molecular chaperone mediated late-stage neuroprotection in the SOD1(G93A) mouse model of amyotrophic lateral sclerosis. PLoS One 8 (8), e73944.

Parakh, S., Atkin, J.D., 2016. Protein folding alterations in amyotrophic lateral sclerosis. Brain. Res. 1648 (B), 633–649 Pt.

Peng, R., Gallwitz, D., 2002. Sly1 protein bound to Golgi syntaxin Sed5p allows assembly and contributes to specificity of SNARE fusion complexes. J. Cell. Biol. 157 (4), 645–655.

Renna, M., Schaffner, C., Winslow, A.R., Menzies, F.M., Peden, A.A., Floto, R.A., Rubinsztein, D.C., 2011. Autophagic substrate clearance requires activity of the syntaxin-5 SNARE complex. J. Cell. Sci. 124 (3), 469–482 Pt.

Sahlin, K., Broberg, S., Ren, J.M., 1989. Formation of inosine monophosphate (IMP) in human skeletal muscle during incremental dynamic exercise. Acta. Physiol. Scand. 136 (2), 193–198.

Scotter, E.L., Chen, H.J., Shaw, C.E., 2015. TDP-43 proteinopathy and ALS: insights into disease mechanisms and therapeutic targets. Neurotherapeutics 12 (2), 352–363.

Seminary, E.R., Sison, S.L., Ebert, A.D., 2018. Modeling protein aggregation and the heat shock response in ALS iPSC-derived motor neurons. Front. Neurosci. 12, 86.

Sharp, P.S., Akbar, M.T., Bouri, S., Senda, A., Joshi, K., Chen, H.J., Latchman, D.S., Wells, D.J., de Belleroche, J., 2008. Protective effects of heat shock protein 27 in a model of ALS occur in the early stages of disease progression. Neurobiol. Dis. 30 (1), 42–55.

Shen, S., Park, J.W., Lu, Z.X., Lin, L., Henry, M.D., Wu, Y.N., Zhou, Q., Xing, Y., 2014. rMATS: robust and flexible detection of differential alternative splicing from replicate RNA-Seq data. Proc. Natl. Acad. Sci. U S A 111 (51), E5593–E5601.

van Es, M.A., Hardiman, O., Chio, A., Al-Chalabi, A., Pasterkamp, R.J., Veldink, J.H., van den Berg, L.H., 2017. Amyotrophic lateral sclerosis. Lancet 390 (10107), 2084–2098.

van Rheenen, W., Shatunov, A., Dekker, A.M., McLaughlin, R.L., Diekstra, F.P., Pulit, S.L., van der Spek, R.A., Vosa, U., de Jong, S., Robinson, M.R., Yang, J.,

Fogh, I., van Doormaal, P.T., Tazelaar, G.H., Koppers, M., Blokhuis, A.M., Sproviero, W., Jones, A.R., Kenna, K.P., van Eijk, K.R., Harschnitz, O., Schellevis, R.D., Brands, W.J., Medic, J., Menelaou, A., Vajda, A., Ticozzi, N., Lin, K., Rogelj, B., Vrabec, K., Ravnik-Glavac, M., Koritnik, B., Zidar, J., Leonardis, L., Groselj, L.D., Millecamps, S., Salachas, F., Meininger, V., de Carvalho, M., Pinto, S., Mora, J.S., Rojas-Garcia, R., Polak, M., Chandran, S., Colville, S., Swingler, R., Morrison, K.E., Shaw, P.J., Hardy, J., Orrell, R.W., Pittman, A., Sidle, K., Fratta, P., Malaspina, A., Topp, S., Petri, S., Abdulla, S., Drepper, C., Sendtner, M., Meyer, T., Ophoff, R.A., Staats, K.A., Wiedau-Pazos, M., Lomen-Hoerth, C., Van Deerlin, V.M., Trojanowski, J.Q., Elman, L., McCluskey, L., Basak, A.N., Tunca, C., Hamzeiy, H., Parman, Y., Meitinger, T., Lichtner, P., Radivojkov-Blagojevic, M., Andres, C.R., Maurel, C., Bensimon, G., Landwehrmeyer, B., Brice, A., Payan, C.A., Saker-Delye, S., Durr, A., Wood, N.W., Tittmann, L., Lieb, W., Franke, A., Rietschel, M., Cichon, S., Nothen, M.M., Amouyel, P., Tzourio, C., Dartigues, J.F., Uitterlinden, A.G., Rivadeneira, F., Estrada, K., Hofman, A., Curtis, C., Blauw, H.M., van der Kooi, A.J., de Visser, M., Goris, A., Weber, M., Shaw, C.E., Smith, B.N., Pansarasa, O., Cereda, C., Del Bo, R., Comi, G.P., D'Alfonso, S., Bertolin, C., Sorarù, G., Mazzini, L., Pensato, V., Gellera, C., Tiloca, C., Ratti, A., Calvo, A., Moglia, C., Brunetti, M., Arcuti, S., Capozzo, R., Zecca, C., Lunetta, C., Penco, S., Riva, N., Padovani, A., Filosto, M., Muller, B., Stuit, R.J., Registry, P., Group, S., Registry, S., Consortium, F.S., Consortium, S., Group, N.S., Blair, I., Zhang, K., McCann, E.P., Fifita, J.A., Nicholson, G.A., Rowe, D.B., Pamphlett, R., Kiernan, M.C., Grosskreutz, J., Witte, O.W., Ringer, T., Prell, T., Stubendorff, B., Kurth, I., Hubner, C.A., Leigh, P.N., Casale, F., Chio, A., Beghi, E., Pupillo, E., Tortelli, R., Logroscino, G., Powell, J., Ludolph, A.C., Weishaupt, J.H., Robberecht, W., Van Damme, P., Franke, L., Pers, T.H., Brown, R.H., Glass, J.D., Landers, J.E., Hardiman, O., Andersen, P.M., Corcia, P., Vourc'h, P., Silani, V., Wray, N.R., Visscher, P.M., de Bakker, P.I., van Es, M.A., Pasterkamp, R.J., Lewis, C.M., Breen, G., Al-Chalabi, A., van den Berg, L.H., Veldink, J.H., 2016. Genome-wide association analyses identify new risk variants and the genetic architecture of amyotrophic lateral sclerosis. Nat. Genet. 48 (9), 1043–1048.

van Rheenen, W., van der Spek, R.A.A., Bakker, M.K., van Vugt, J., Hop, P.J., Zwamborn, R.A.J., de Klein, N., Westra, H.J., Bakker, O.B., Deelen, P., Shireby, G., Hannon, E., Moisse, M., Baird, D., Restuadi, R., Dolzhenko, E., Dekker, A.M., Gawor, K., Westeneng, H.J., Tazelaar, G.H.P., van Eijk, K.R., Kooyman, M., Byrne, R.P., Doherty, M., Heverin, M., Al Khleifat, A., Iacoangeli, A., Shatunov, A., Ticozzi, N., Cooper-Knock, J., Smith, B.N., Gromicho, M., Chandran, S., Pal, S., Morrison, K.E., Shaw, P.J., Hardy, J., Orrell, R.W., Sendtner, M., Meyer, T., Basak, N., van der Kooi, A.J., Ratti, A., Fogh, I., Gellera, C., Lauria, G., Corti, S., Cereda, C., Sproviero, D., D'Alfonso, S., Soraru, G., Siciliano, G., Filosto, M., Padovani, A., Chio, A., Calvo, A., Moglia, C., Brunetti, M., Canosa, A., Grassano, M., Beghi, E., Pupillo, E., Logroscino, G., Nefussy, B., Osmanovic, A., Nordin, A., Lerner, Y., Zabari, M., Gotkine, M., Baloh, R.H., Bell, S., Vourc'h, P., Corcia, P., Couratier, P., Millecamps, S., Meininger, V., Salachas, F., Mora Pardina, J.S., Assialioui, A., Rojas-Garcia, R., Dion, P.A., Ross, J.P., Ludolph, A.C., Weishaupt, J.H., Brenner, D., Freischmidt, A., Bensimon, G., Brice, A., Durr, A., Payan, C.A.M., Saker-Delye, S., Wood, N.W., Topp, S., Rademakers, R., Tittmann, L., Lieb, W., Franke, A., Ripke, S., Braun, A., Kraft, J., Whiteman, D.C., Olsen, C.M., Uitterlinden, A.G., Hofman, A., Rietschel, M., Cichon, S., Nothen, M.M., Amouyel, P., Consortium, S., Consortium, P., Consortium, S., Consortium, S., Traynor, B.J., Singleton, A.B., Mitne Neto, M., Cauchi, R.J., Ophoff, R.A., Wiedau-Pazos, M., Lomen-Hoerth, C., van Deerlin, V.M., Grosskreutz, J., Roediger, A., Gaur, N., Jork, A., Barthel, T., Theele, E., Ilse, B., Stubendorff, B., Witte, O.W., Steinbach, R., Hubner, C.A., Graff, C., Brylev, L., Fominykh, V., Demeshonok, V., Ataulina, A., Rogelj, B., Koritnik, B., Zidar, J., Ravnik-Glavac, M., Glavac, D., Stevic, Z., Drory, V., Povedano, M., Blair, I.P., Kiernan, M.C., Benyamin, B., Henderson, R.D., Furlong, S., Mathers, S., McCombe, P.A., Needham, M., Ngo, S.T., Nicholson, G.A., Pamphlett, R., Rowe, D.B., Steyn, F.J., Williams, K.L., Mather, K.A., Sachdev, P.S., Henders, A.K., Wallace, L., de Carvalho, M., Pinto, S., Petri, S., Weber, M., Rouleau, G.A., Silani, V., Curtis, C.J., Breen, G., Glass, J.D., Brown Jr., R.H., Landers, J.E., Shaw, C.E., Andersen, P.M., Groen, E.J.N., van Es, M.A., Pasterkamp, R.J., Fan, D., Garton, F.C., McRae, A.F., Davey Smith, G., Gaunt, T.R., Eberle, M.A., Mill, J., McLaughlin, R.L., Hardiman, O., Kenna, K.P., Wray, N.R., Tsai, E., Runz, H., Franke, L., Al-Chalabi, A., Van Damme, P., van den Berg, L.H., Veldink, J.H., 2021. Common and rare variant association analyses in amyotrophic lateral sclerosis identify 15 risk loci with distinct genetic architectures and neuron-specific biology. Nat. Genet. 53 (12), 1636–1648.

Vasta, R., Chia, R., Traynor, B.J., Chio, A., 2022. Unraveling the complex interplay between genes, environment, and climate in ALS. EBioMedicine 75, 103795.

Verma, S., Khurana, S., Vats, A., Sahu, B., Ganguly, N.K., Chakraborti, P., Gourie-Devi, M., Taneja, V., 2022. Neuromuscular Junction Dysfunction in Amyotrophic Lateral Sclerosis. Mol. Neurobiol. 59 (3), 1502–1527.